*Jahangirnagar University*
*Journal of Geospatial Sciences*
*Volume 1, 2025; DOI: [https://doi.org/10.59185/jgs.v1i1.271](https://doi.org/10.59185/jgs.v1i1.271)*

*Technical Note*

# Impact of Land Use Land Cover Changes on Land Surface Temperature in Jessore District of Bangladesh: A Remote Sensing Approach

**Md. Tarequl Islam [1*], Md. Adil Shahriar [2], Md. Munir Mahmud [3]**

[1] Section Officer (COE), Bangladesh Army University of Science and Technology Khulna, Khulna - 9204, Bangladesh
[2] Research Officer, Geospatial Research and Development Lab, Eutech Systems Limited, Dhaka-1212, Bangladesh
[3] Assistant Professor, Institute of Remote Sensing and GIS, Jahangirnagar University, Bangladesh

**Corresponding Author: tareqccpc@gmail.com*

**Abstract**

*Rapid urbanization puts a lot of strain on local climate systems, with land use and land cover (LULC) changes directly influencing land surface temperature (LST) patterns. This study uses multi-temporal Landsat 7 ETM+ and Landsat 8 OLI satellite imagery for the year 2000, 2010, and 2020 to investigate the relationship between LULC changes and LST fluctuations in Jessore, Bangladesh. Analysis indicated significant urban growth throughout the two-decade span, with built-up areas increasing by 2% while agricultural land and vegetation cover declined by 2% and water bodies contracted by 1%. The analysis of LST revealed that the built-up area experienced the highest temperatures then came bare land, vegetation, agricultural, and water bodies respectively. Throughout the duration of the research, the overall LST rose by 3°C, with the most noticeable warming occurring in populated regions. The study demonstrates that the decrease in vegetation cover and the spread of impervious surfaces are the major factors leading to the increase in surface temperatures in Jessore. The research LULC-LST profiles also showed that the degree of heat was highest in populated regions and lowest in water bodies. The study demonstrates that the vegetation cover in the study area is decreasing, and the non-evaporating surfaces are rising, and the surface temperature is escalating remarkably. The findings are critical in making climate-resilient policies in urban planning and the strategies of mitigating the urban heat island impact in developing cities in Bangladesh.*

**Keywords:** LULC, Kappa statistics, LST, NDVI, Jashore district

## 1 Introduction

Residents actively contribute to the economic development and regional exploitation of their city. (Weng., 2001). This change in LULC has an effect on LST and the city climate. (Herold., 2003). Due to their close connection, land cover (LC) and land use (LU) are frequently researched together despite their distinct meanings. Land cover (LC) and land use (LU) are often studied as a combination, though they have different implications because of their strong connection. LC is the area of the earth that is covered with natural resources and other inbuilt features (Fan C., 2017). In contrast, LU refers to the part humans cover for their purposes (Verburg., 2009). Increasing urbanization decreases carbon absorption by reducing the region's forested land, vegetation, and aquatic bodies. (Kumar et al., 2012; Thakur et al., 2019). As a result of pollution and urbanization, land surface temperatures will likely rise dramatically by 2050 in most regions, particularly in emerging nations. (Hua et al., 2018). LULC has the most influence over LST (Kumar & Shekhar, 2015). Several LULCs, including agriculture and crop production, affect the geographic distribution of atmospheric energy for cooling and moisturizing the area around them (Feng et al., 2018). The number of urban heat islands is rising, which harms the ecosystem and quality of city life. This problem is caused by modifying LCLU and increasing built-up territory (Bao et al., 2016; Mallick et al., 2013). More agricultural land is being converted into urban sprawl due to the rising land needs for housing, manufacturing, and infrastructure (Wadduwage et al., 2017). These characteristics are associated with the urban-rural biota, land cover and socio-economic variables. Emerging countries often have cities that are characterized by different urban development that are incompatible with regional objectives and policies. For instance, Jessore is a rapidly growing city in the Khulna division. It also increases the level of its temperature so that it grows the settlement fast. In its turn, this has made it necessary to evaluate the way these human-based transformations have affected the plants in the city. Therefore, we wish to determine the effects of LULC variations in Jessore over the past two decades on sea level rise. (Akomolafe, 2022). The land use and land cover (LULC) change is also one of the influential factors on the environment and the climate of the earth. To understand these changes with time, remote sensing methods have been important in monitoring and analyzing them. The population of Bangladesh is expanding quite quickly, which leads to the demand of land and thus LULC changes. In this research, remote sensing techniques are employed in examining the impact of the LULC changes on the LST at the Bangladeshi locality of Jessore. The issue of LULC transformations has emerged as a major concern across the globe since it has a lot of effects on the environment, including LST. As human activities, mainly urbanization, agricultural expansion, and others, have increased over time, LULC has changed significantly, causing change in LST. The LULC changes and effects on LST have been analyzed and remotely sensed methods have been indicated to be useful. Focusing on the main drivers of LULC changes and its effects on temperature, a large number of research have been carried out in the world evaluating the relationship between LULC changes and LST (Fan, 2017).

# 2 Data and Methods

## 2.1 Study Area

Jessore district (Figure 1) borders Jhinaidah on the north, Narail and Magura on the east, Khulna and Satkhira on the south, and India on the west. The total area of the district is 2605.89 km². The district lies within the north latitudes 22°48' to 23°22' with east longitudes 88°51' to 89°34'. The maximum and minimum annual temperatures are 36°C and 10°C, respectively. The rainfall is 1,537 mm per annum. It is constructed in 1781 and recreated in 1984. The district is comprised of eight upazilas, 92 unions, 1,329 mauzas, 1,419 villages and eight municipalities. In the year 1786, Jessore was the first district of independent Bengal. The west Ganges River floodplain is the area that the district belongs to, and the highland and medium-highland areas are the prevailing ones. The most typical varieties of floodplain soil are dark gray and calcareous brown soils with a pH that is somewhat alkaline and poor in organic matter. The fertility is not very high, although both cereals and vegetables are well adapted in the area. Jessore is primarily agricultural land with rice, sugarcane and dates being large agricultural fields. In Bangladesh, farming is rather active, and the amount of bare land is minimal as well as built-up lands are not so large.

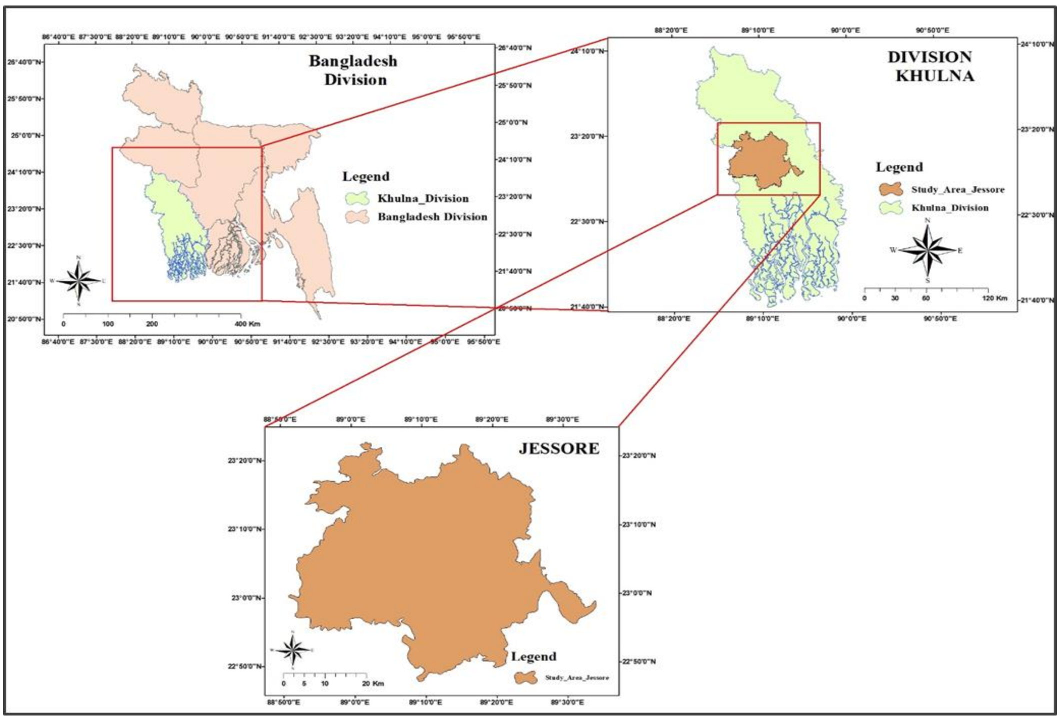


**Figure 1:** Study Area Jessore District of Bangladesh (Source: Compiled by author)

## 2.2 Data Sources

The study employed Landsat 7 Enhanced Thematic Mapper (ETM+) and Landsat 8 Operational Land Imager satellite pictures from 2000, 2010, and 2020 that were obtained from the US Geological Survey website. The number of the row is 044 and the mode of the path is 138. The spatial resolution of every picture is 30m. The Landsat images (Level 1 Terrain Corrected product) were projected onto UTM zone 45 North using the WGS-84 datum. To avoid seasonal instability, the Landsat photos were taken in the same month. Illustrations were made in cloud-free settings throughout the late fall months of December, January, and February to produce LULC and LST distribution maps. Images were processed, categorized, and picture alterations were detected using ArcMap 10.8. The methodology of this study was outlined through a flow chart (Figure 2) and Google Earth Pro is used for data identification. Microsoft Excel was employed for area calculations. The research followed a quantitative approach, which involves systematic empirical investigation of observable phenomena through the application of statistical, mathematical, or computational techniques. The primary objective of quantitative research is to generate numerical data that can be generalized across different groups or utilized to explain underlying phenomena.

A long temporal context of 20 years (2000-2020) allows for integral evaluation of urban transition processes and environmental changes in Jessore. The long temporal duration comprises full urban development phase cycles with enough temporal resolution to detect slow environmental changes that cannot be inferred from shorter study intervals. The 20-year analysis frame is consistent with conventional urban planning cycles that yield strong trend detection and statistical significance in the detection of transitions in land use and thermal environment modifications, offering essential information for climate adaptation measures and sustainable urban development planning.

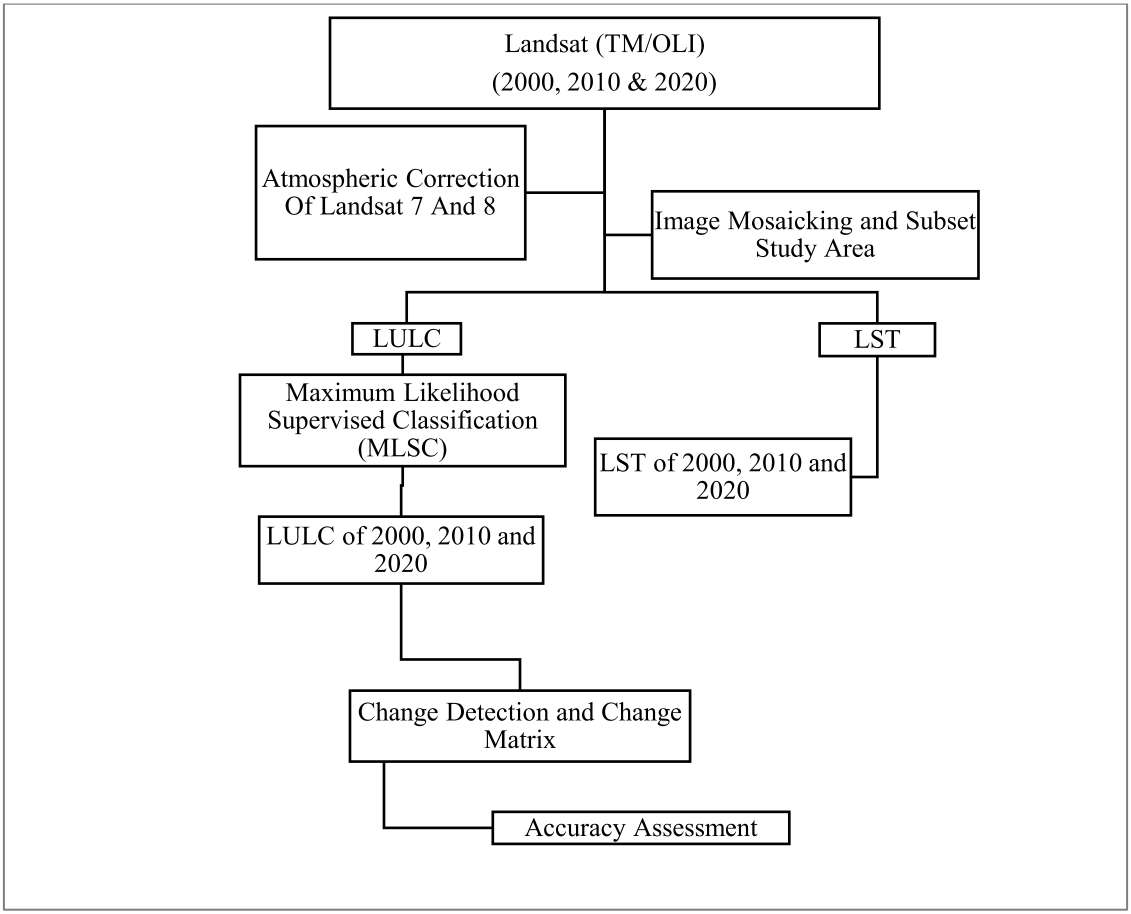


**Figure 2:** The Flow chart of Methodology

## 2.3 Method

Quantitative methodologies were used to identify the LULC and its effects on the land surface and individuals. Moreover, this technique was used to develop a general picture of the fluctuation of temperature at the various times of the year. The analysis of settlement of the various years and change was carried out using geostatistical tools in this research. Secondary literature is also used to gain an insight into the effects of LULC. The population secondary data was used as a quality parameter in this research. A vast amount of such data is contained in the Bangladesh Bureau of Statistics (BBS). Details of the satellite images and sensors used in this study are presented in (Table 1) (Source: USGS Landsat Mission).

**Table 1:** Satellite and Sensor Details

| Satellite Image | Data Acquisition Time | Sensor | Path/Row | Bands | Spectral range (Wavelength µm) | Spatial resolution (m) |
|---|---|---|---|---|---|---|
| Landsat 7 | 17th November, 2000 & 16th November, 2010 | ETM (Enhanced Thematic Mapper Plus) | 138/044 | 1 | .45 - .52 µm | 30 |
| | | | | 2 | .52 - .60 µm | 30 |
| | | | | 3 | .63 - .69 µm | 30 |
| | | | | 4 | .77 - .90 µm | 30 |
| | | | | 5 | 1.55 - 1.75 µm | 30 |
| | | | | 6 | 10.40 - 12.50 µm | 60 |
| | | | | 7 | 2.08 - 2.35 µm | 30 |
| | | | | 8 | .52 - .90 µm | 15 |
| Landsat 8 | 16th November, 2020 | Operational Land Imager (OLI) | 138/044 | 1 | .43 - .45 µm | 30 |
| | | | | 2 | .45 - .51 µm | 30 |
| | | | | 3 | .53 - .59 µm | 30 |
| | | | | 4 | .64 - .67 µm | 30 |
| | | | | 5 | .85 - .88 µm | 30 |
| | | | | 6 | 1.57 - 1.65 µm | 30 |
| | | | | 7 | 2.11 - 2.29 µm | 30 |
| | | | | 8 | .50 - .68 µm | 30 |
| | | | | 9 | 1.36 - 1.38 µm | 30 |
| | | | | 10 (TRIS 1) | 10.60-11.19 µm | 100 resampled to 30 |
| | | | | 11 (TRIS 1) | 11.50-12.51 µm | 100 resampled to 30 |

### 2.4 Classification of Land Use / Land Cover

The LULC is classified into urban, aquatic, forested and open terrain. Maximum likelihood supervised classification (MLSC) is used to classify satellite pictures based on selected training areas. The overall accuracy, Kappa coefficient, and accuracy confirmation were considered as standard measures to assess the land use classification accuracy. Kafy et al. (2018 and 2019) explain the most common application of MLSC in the classification of images. Using Google Earth images of 350 randomly chosen locations, the validity of both classified maps was established.

### 2.5 Land Surface Temperature (LST) Derivation

A remote sensing inversion model that simulates LST was demonstrated using the thermal infrared band of satellite pictures (Min et al., 2019). Digital Numbers (DN) of the thermal bands (Band 6 in Landsat 5 TM and Bands 10 in Landsat 8 TIRS) were used to calculate the LST. In the initial stage, spectral radiance (Lλ) of the Landsat 5 TM and Landsat 8 TIRS bands were calculated by using equations (i) and (ii) (Roy et al., 2016), respectively.

Finally, $L_\lambda$ was used to determine the LST in degrees celsius using equation (iii) (Roy et al., 2016).

$$L_\lambda(Landsat\ 7\ ETM) = L_{min} + \frac{L_{max} - L_{min}}{Qcal\ + Qcal_{\ min}} \times DN \text{.......... (i)}$$

$$L_\lambda(Landsat\ 8\ OLI) = ML \times DN + AL \text{......................... (ii)}$$

$$LST = \frac{T_B}{1+\left\{\left(\lambda\times\frac{T_B}{T_B}\right)\times lnln\ (\varepsilon)\right\}} - 273.15 \text{ ............................ (iii)}$$

In which ML (0.0003342) is a band-specific multiplicative rescaling factor, and AL (0.1) is a band-specific additive rescaling factor. (Kamran et al., 2015; Sholihah and Shibata, 2019). Landsat TM, L$min$, and L$max$ values were taken from a satellite's metadata file. The wavelength of the electromagnetic interference that is released is 11.5 m. The radiance constant (**ρ**) used in equation (iv) as follows:

$$\rho = h \times \frac{c}{\sigma} \quad = 1.438 \times 10^{-2} \quad mK \text{ ............................ (iv)}$$

where, h denotes Plank's constant which is equal to 6.626×$10^{-34}$ Js in equation 4 (Minnett and Barton, 2009), c indicates the speed of light, which is equal to 2.998×108 $ms^{-2}$ and $\sigma$ is the Boltzmann constant (5.67×10-8 $Wm^{2}\,k^{-4}$ = 1.38 ×$10^{-23}\,JK^{-1}$). $\varepsilon$ is the land surface emissivity which is scaled between 0.97 and 0.99.

$$T_B = \frac{K_2}{lnln\left(\frac{K_1}{L_\lambda}+1\right)} \text{ ............................ (v)}$$

where $T_B$ is the satellite brightness temperature in equation (v) and $K_1$ and $K_2$ constant values for 1 ($K_1$ and $K_2$ values for Landsat-7 are 607.7 and 1260.6, respectively.) Landsat-8 values are 774.9 and 1321.07, respectively (Minnett and Barton, 2009).

# 3 Results and Discussions

## 3.1 Land Use and Land Cover

LULC (Figure 3) shows maps of 2000, 2010 and 2020 which were produced using classified imagery. The percentage distribution of different Land Use and Land Cover (LULC) classes for the study years are presented in (Table 2). LULC maps show that in 2000-2020, the built-up areas will grow sharply (2%), but in contrast, the vegetation and agricultural lands will decrease sharply ( -2%). There was a small increase and decrease in grassland (20%) and water areas (-1%). Also, we can observe that it has undergone a reduction in vegetation and water land by 6% and 14, respectively. In 2000 the area under water bodies was 44.90 km$^2$ but will decrease to just 29.04 km$^2$ in 2020. In 2000, the developed space within the city centre (522.67 km$^2$) was small. The total developed land area increased drastically in 2020 encroaching on water bodies and plant life. As of 2020, the rapidly expanding urbanized zone (55.95 km$^2$) was scattered across the suburban and outskirts boundaries. The land was largely involved in vegetation cover and agriculture over the years although this proportion declined over the period 2000-2020 to 1047442.16 km$^2$. Most of the agricultural and vegetation land initially turned into bare land and then developed into populated areas. Consequently, the raw land and grassland expanded slowly in the period between 2000 and 2020, and this improved to 864.85 km$^2$ to 1385.85 km$^2$.

**Table 2.** LULC Distribution

| **Year** | **2000** | | **2010** | | **2020** | | **Change (%)** | | |
|---|---|---|---|---|---|---|---|---|---|
| **Classes** | **Area in Km$^2$** | **%** | **Area in Km$^2$** | **%** | **Area in Km$^2$** | **%** | **Year 2000 To 2010** | **Year 2010 To 2020** | **Year 2000 To 2020** |
| Agricultural Land | 156.75 | 6% | 277.12 | 11% | 99.51 | 4% | 5% | -7% | -2% |
| Aqua Land | 168.28 | 7% | 136.11 | 5% | 25.70 | 1% | -2% | -4% | -6% |
| Built-up Land | 522.67 | 21% | 452.54 | 18% | 579.95 | 23% | -3% | 5% | 2% |
| Grass Land | 864.84 | 34% | 355.00 | 14% | 1385.84 | 54% | 20% | 40% | 20% |
| Vegetation | 787.76 | 31% | 1242.09 | 49% | 425.17 | 17% | 18% | -32% | -14% |
| Water Body | 44.90 | 2% | 82.41 | 3% | 29.04 | 1% | 1% | -2% | -1% |

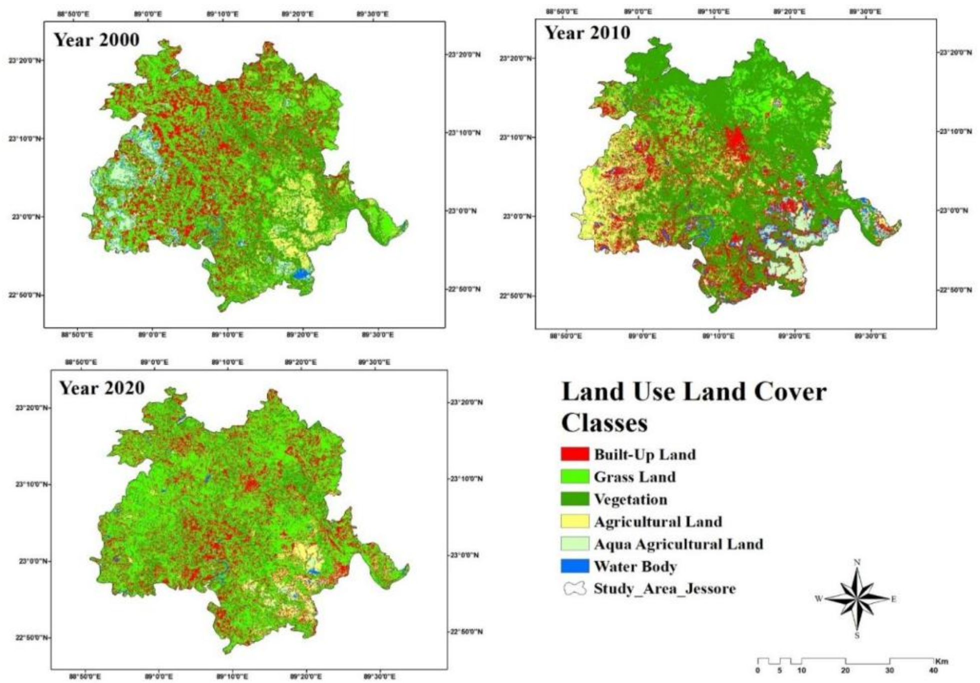


**Figure 3:** Land Use Land Cover Map

### 3.2 Validation of Classified LULC Maps

One way to assess the accuracy of an estimate is to compare it against gold-standard data from remote sensing. According to Lu and Weng (2007), the number of training sets and the degree to which they are representative are crucial for image classification. Geographic data must be collected at a time consistent with the historical context. (Wondrade et al. 2014). As auxiliary data, digital topographic maps at a scale of 1: 5,000, aerial photographs from 2005 at a scale of 1: 5,000, GPS point reference data, Google Earth observations, visual interpretation, and our local knowledge were used to improve the classification accuracy of each image. (Zhang et al. 2013; Li et al. 2012). The accuracy was evaluated using reference statistics. (Yuan et al. 2005). The precision of the benchmarks for the stratified random sampling method was assessed. (Xiao and Weng 2007). The confusion matrix of each LULC map, according to Ji and Niu (2014), reveals its veracity. (Ghebrezgabher et al. 2016). The accuracy of the producer, the user, and the Kappa statistics in implementing reference points has been evaluated based on classification results. (Churches et al. 2014). To evaluate their accuracy, the categorization results were appended to the reference data.

The accuracy evaluation of the classification of the LULC in the years 2000, 2010, and 2020 shows a consistent decline in classification reliability over the years (Table 3). The overall accuracy in 2000 was 90% with a Kappa coefficient of 0.88, meaning that there existed strong agreement between reference and classified data. The user's accuracy ranged from 80% (water bodies) to 100% (all other classes), and the producer's accuracy levels were high in general with the least being the water bodies (83%). The overall accuracy in 2010 fell marginally to 86% with a Kappa coefficient of 0.84. The user's accuracy remained stable across most of the classes, with vegetation decreasing significantly to 80%. The producer's accuracy was also variable with agricultural land and aquacultural land decreasing to 83%. By the year 2020, the classification became even more inaccurate at 80% overall with a Kappa coefficient of 0.76. The user's accuracy remained spotless in grassland and vegetation but fell significantly in agricultural land (80%), aquacultural land (80%), and water bodies (60%). Likewise, the producer's accuracy of the water bodies and the aquacultural land fell to 67%. The results indicate that although the classification procedure was strong in the past, the classification over the period weakened, with the decrease in classification reliability being due largely to the increase in landscape heterogeneity and spectral confusion within the classes.

**Table 3.** Accuracy assessment

| | User accuracy | | | | | | Producer Accuracy | | | | | | | |
|---|---|---|---|---|---|---|---|---|---|---|---|---|---|---|
| **Year** | **Built-up Land** | **Grassland** | **Vegetation** | **Agricultural land** | **Aqua Agricultural Land** | **Water Body** | **Built-up Land** | **Grassland** | **Vegetation** | **Agricultural land** | **Aqua Agricultural Land** | **Water Body** | **Overall Accuracy** | **Kappa Coefficient** |
| **2000** | 100% | 100% | 100% | 100% | 100% | 80% | 100% | 71.40% | 100% | 100% | 0.833 | 100% | 90% | 0.88 |
| **2010** | 60% | 100% | 80% | 100% | 100% | 80% | 100% | 71.40% | 100% | 83% | 83% | 100% | 86% | 0.84 |
| **2020** | 60% | 100% | 100% | 80% | 80% | 60% | 100% | 71% | 100% | 67% | 67% | 100% | 80% | 0.76 |

### 3.3 Change Detection of LULC

LULC change analysis during the period from 2000 to 2020 suggests significant changes across the classes (Table 4) and (Figure 4). Built-up land expanded by 91.88 km² (24%), predominantly at the cost of agricultural and vegetation land. The highest gain (370.94 km², 14%) was observed in vegetation, but the highest loss (37%) was also registered in this land cover type, indicating high spatial redistribution. Agricultural land and aquacultural land registered moderate changes with net gain in the order of 78.1 km² and 156.34 km² respectively, but with losses of 8% and 10%. Water bodies remained stable with net gain of only 31.14 km². The urban expansion and vegetation dynamics remained the highest driver of the land cover change during the study duration. The change variations in land use and land cover from 2000 to 2020 over the study period are illustrated in (Figure 5). Map showing unchanged, decreased, and increased areas of the study region illustrates the spatial distribution of land cover transitions, identifying zones of stability, loss, and expansion between the analysed years (Figure 6).

**Table 4:** Change Matrix Transform Rate of LULC from 2000 To 2020

| **Changes** | **Built-up Land** | **Grassland** | **Vegetation** | **Agricultural land** | **Aqua-Agricultural Land** | **Water Body** |
|---|---|---|---|---|---|---|
| Area Change To ($Km^2$) | 91.88 | 0.00 | 370.95 | 78.1 | 156.35 | 31.14 |
| Area Converted from ($Km^2$) | 307.20 | 343.86 | 579.20 | 117.41 | 162.27 | 38.0 |
| Transform Rate (%) | 29.90 | 0.00 | 64.05 | 66.53 | 96.34 | 81.9 |

| Changes | Built-up Land | Grassland | Vegetation | Agricultural land | Aqua-Agricultural Land | Water Body |
|---|---|---|---|---|---|---|
| Increase Rate (%) | 24% | 56% | 14% | 4% | 1% | 1% |
| Decrease Rate (%) | 20% | 22% | 37% | 8% | 10% | 2% |

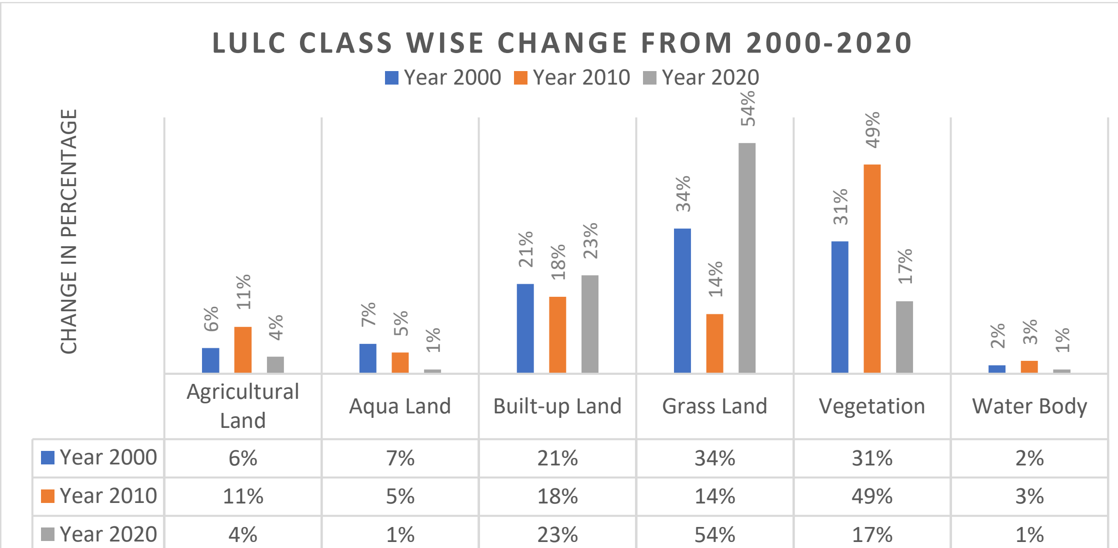


**Figure 4:** LULC class wise change from 2000-2020

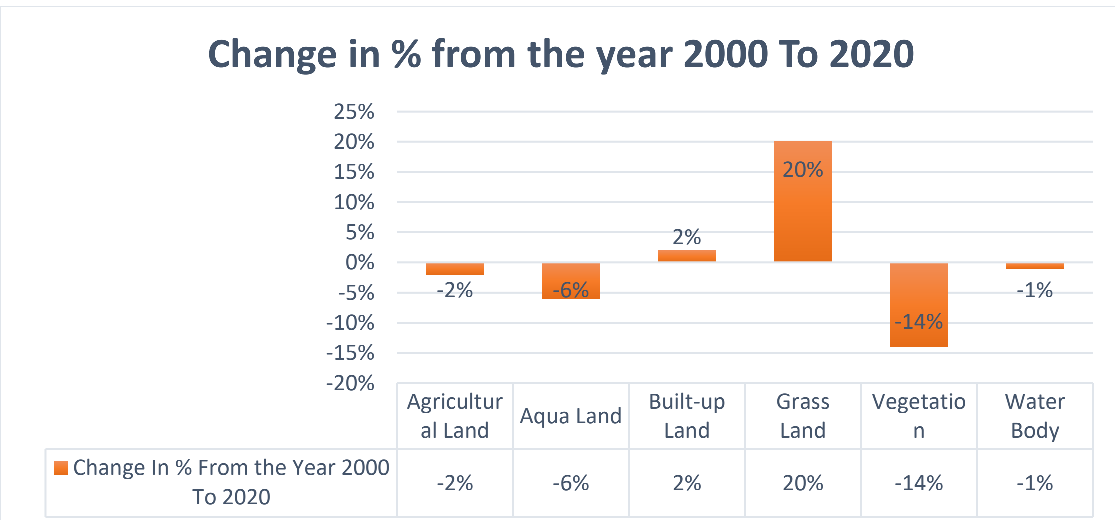


**Figure 5:** Change in Percentage in LULC Classes (2000–2020)

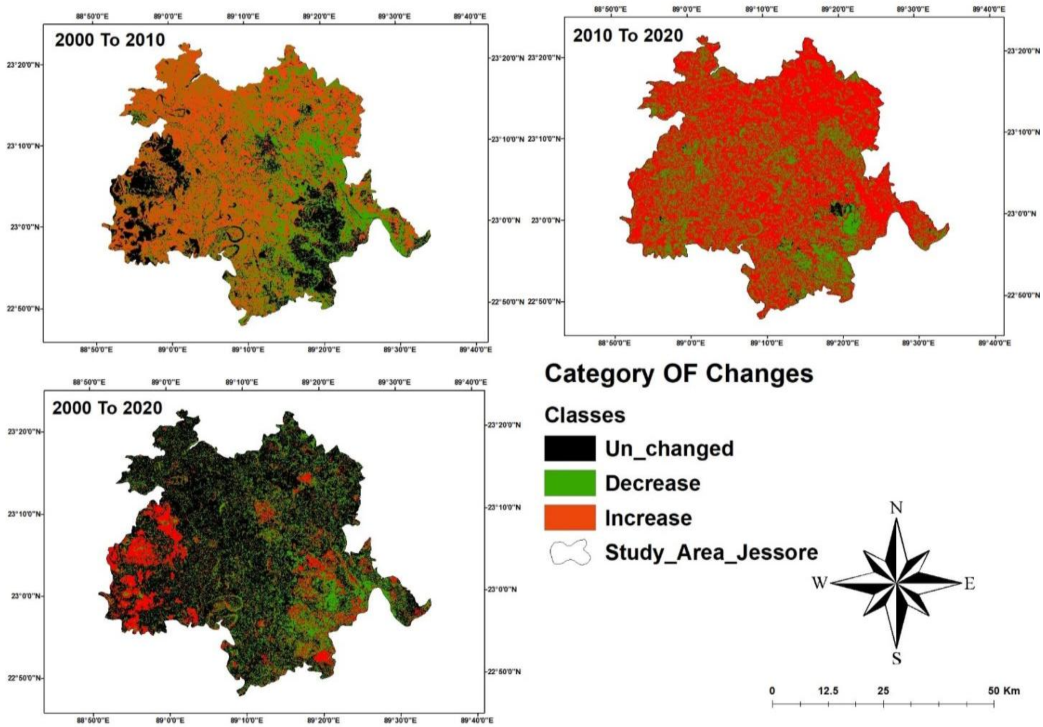


**Figure 6:** Showing the Changes in Study Area (Source: Compiled by author)

### 3.4 Change in Land Surface Temperature

Table 5 present the temporal variation of LST for the years 2000, 2010, and 2020. In the spatial distribution maps (Figure 7), red shades represent higher temperatures, while blue shades indicate lower LST values. The spatial concentration and temporal progression of LST reflect the rapid transformation of LULC categories during the study period. The typical temperature ranges were 21–31 °C in 2000, 18–25 °C in 2010, and 20–31 °C in 2020. In 2000, approximately 39% of the area experienced temperatures between 23 °C and 24 °C, which decreased to 35% by 2020. Central urban areas were particularly vulnerable to elevated LST, with 36% of the area exceeding 20–21 °C in 2010. On average, LST increased by nearly 3°C from 2000 to 2020, although this rise is based on mathematical estimation. Spatially, LST increased in the northwest of the study area due to urban growth, reduced vegetation, and declining water bodies, whereas in the southeast it decreased, supported by greater vegetation cover and extensive agricultural land.

**Table 5:** Area temperature wise and percentage (Source: Compiled by author)

| Year | 2000 | | 2010 | | | 2020 | | |
|---|---|---|---|---|---|---|---|---|
| **Temp** | **Area Km²** | **%** | **Temp** | **Area Km²** | **%** | **Temp** | **Area Km²** | **%** |
| 21-23 | 244.61 | 10% | 18-19 | 265.83 | 10% | 20-22 | 661.84 | 26% |
| 23-24 | 987.33 | 39% | 19-20 | 484.51 | 19% | 22-23 | 896.81 | 35% |
| 24-25 | 847.01 | 33% | 20-20 | 592.21 | 23% | 23-24 | 590.06 | 23% |
| 25-26 | 401.57 | 16% | 20-21 | 904.76 | 36% | 24-25 | 315.68 | 12% |
| 26-31 | 64.62 | 3% | 21-24 | 297.84 | 12% | 25-30 | 80.79 | 3% |
| **Total** | **2545.13** | | **Total** | **2545.16** | | **Total** | **2545.18** | |

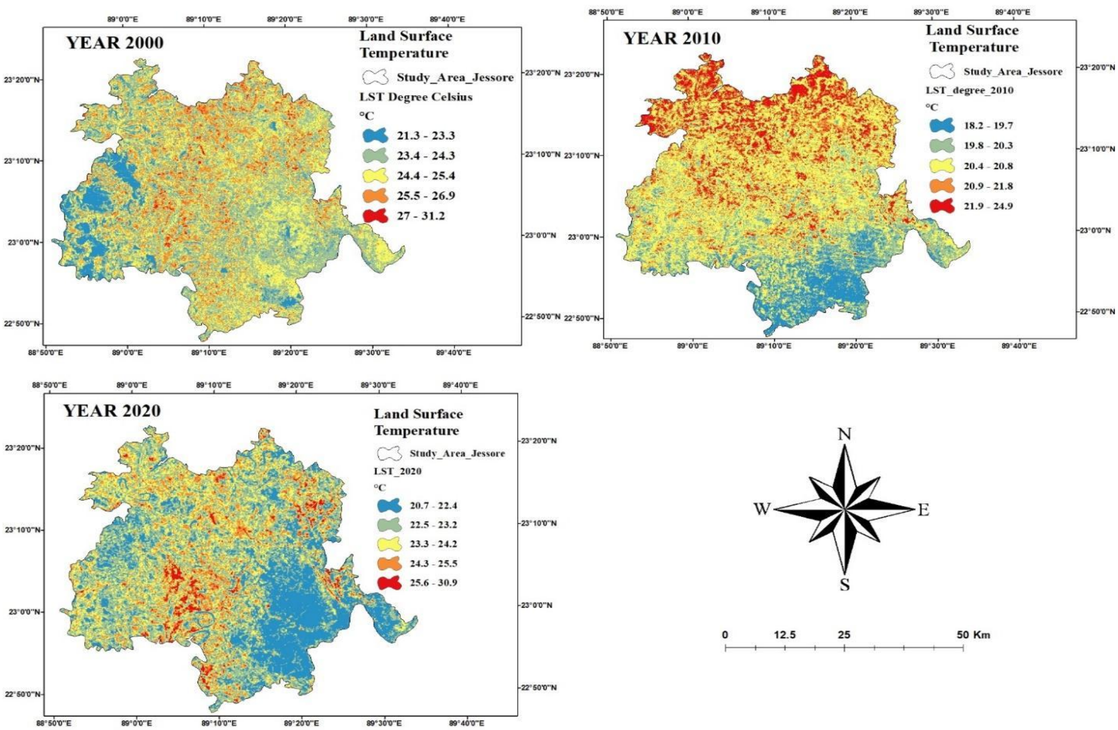


**Figure 7:** Yearly Distribution LST Value of the Study Area

### 3.5 Validation of Estimated LST

The simplest way for obtaining the LST is from the thermal bands in Landsat 7 ETM+ and Landsat 8 OLI pictures. Although this is the easiest way for recovering LST, it has certain drawbacks. First and foremost, a clear sky is a crucial necessity for getting precise measurements when employing satellite remote sensing techniques to retrieve LST.

Consequently, cloud coverage may lead to a serious issue. Second, not every surface material has a distinct emissivity measurement rate in each region (Chen et al., 2006; Neteler, 2010). Those issues will lead to an inaccurate LST estimate in the area. Maximum and minimum temperature data were obtained from Bangladesh Meteorological Department (BMD) for the months of November 2000, 2010, and 2020 to validate the LST estimation derived from remotely sensed data. Table 6 shows the difference between the estimated LST and the recorded LST. The variances were estimated using LST estimates from BMD collected data. Positive deviation values indicate that the observed temperature is lower than the estimated temperature, and negative deviation values indicate the opposite.

For the years 2020 (3.27°C) and 2020 (0.38°C), respectively, the maximum and lowest temperature deviations were the highest. In 2010, the temperature ranged from (-1.05°C) to (-3.35°C) at its highest and minimum values. Based on BMD data, the most significant maximum deviation was initially estimated for 2020 (30.80%). In the last 20 years, there has been a 0.33°C and a -0.5°C temperature disparity between remotely sensed estimates and BMD-recorded LST, respectively. Considering all the drawbacks of estimating LST from remote sensing, the difference between expected and recorded LST is acceptable. It can be employed for future analyses like temperature condition and LST simulation indicators anywhere.

**Table 6:** Validation of remotely sensed LST *(Source: BMD & Remote sensed data)*

| | | **2000** | | **2010** | | **2020** | |
|---|---|---|---|---|---|---|---|
| | **Time of Data** | **Max** | **Min** | **Max** | **Min** | **Max** | **Min** |
| **BMD Record Temp** | November (2000, 2010, 2020) | 24.1 | 22.3 | 25.9 | 21.5 | 23.6 | 20.3 |
| **Remote Sensed LST** | | 31.2 | 21.3 | 24.85 | 18.15 | 30.87 | 20.68 |
| **Deviation in °C** | | 7.1 | -1 | -1.05 | -3.35 | 3.27 | 0.38 |
| **Deviation in %** | | 29.46 | -4.48 | -4.05 | -15.58 | 30.80 | 1.87 |

### 3.6 LULC Vs LST Profiles

The remote sensing LST captures the radiative radiation emitted by ground surface which forms part of the rooftops, pavements, vegetated areas, bare soil, and water. The radiative radiation emitted from the ground's surface, which includes vegetated regions, rooftops, bare soil, pavement, and water, is captured by the remote sensing LST. Here 3 cross-sections were created across the study area to illustrate the LULC-wise LST and the mean LST of each type of LULC (Figures 8,9, and 10). The cross-sections of 2 lines (CD and EF) were created in a south-westerly command due to the greater concentrations of LST values in the eastern and southern zones. The overall distribution of the study area in terms of Land Use and Land Cover (LULC) and Land Surface Temperature (LST) is presented in (Table 7).

**Table 7:** Distribution of the study area (LULC and LST)

| Classes | Area In Km$^2$ | Year - 2000 | Year - 2010 | Year - 2020 |
|---|---|---|---|---|
| Built-up | Area in Km$^2$ (%) | 522.67 (21%) | 452.54 (18%) | 579.95 (23%) |
| | Maximum Temperature | 30.54 | 26.88 | 33.0 |
| | Minimum Temperature | 22.85 | 18.16 | 21.0 |
| Grassland | Area in Km$^2$ (%) | 864.84 (34%) | 355.00 (14%) | 1385.85 (54%) |
| | Maximum Temperature | 30.26 | 24.88 | 29.2 |
| | Minimum Temperature | 21.82 | 19.22 | 20.9 |
| Vegetation | Area in Km$^2$ (%) | 787.75 (31%) | 1242.09 (49%) | 425.16 (17%) |
| | Maximum Temperature | 28.8 | 24.88 | 29.2 |
| | Minimum Temperature | 21.82 | 18.16 | 21.0 |
| Agricultural Land | Area in Km$^2$ (%) | 156.74 (6%) | 277.12 (11%) | 99.50 (4%) |
| | Maximum Temperature | 26.4 | 23.35 | 25.0 |
| | Minimum Temperature | 21.83 | 18.70 | 20.7 |
| Aqua Agricultural Land | Area in Km$^2$ (%) | 168.28 (7%) | 136.11 (5%) | 25.69 (1%) |
| | Maximum Temperature | 27.4 | 24.87 | 23.7 |
| | Minimum Temperature | 21.30 | 18.15 | 20.9 |
| Water body | Area in Km$^2$ (%) | 44.89 (2%) | 82.41 (3%) | 29.04 (1%) |
| | Maximum Temperature | 24.5 | 21.9 | 25.7 |
| | Minimum Temperature | 21.30 | 18.16 | 20.8 |

According to the profile, LST in urban centres areas with a preponderance of built-up land was over 31.2°C in 2000, above 26.87°C in 2010, and above 32.9°C in 2020, respectively. For built-up terrain, greater LST readings of > 31.23ºC, > 26.87ºC and > 32.9ºC were also observed in three separate year cross-sections.

The other two land uses (vegetative land and water bodies) had the lowest temperature, which ranges from < 18ºC to <29.2ºC in conjunction with the built-up region and bare land. Table (9) shows the minimum temperatures for 2010 for vegetation and agricultural land (18ºC). and for the years 2000 and 2020 for water bodies (18ºC and 21ºC). The maximum temperature was then measured for the years 2000 and 2020 in populated areas (31.23°C and 30.9°C, respectively), as well as for the year 2010 in populated areas (24.87°C).

### 3.6.1 Profile Line AB Analysis

The profile line AB running across the north region of the study area shows incredible thermal development within the 20 years period. In 2000, the temperature profile was in the form of weak undulating with a varied range of about 22ºC on water bodies (0-5% area) to 26-27 ºC on agricultural areas (10-15% area) with gradual decrease to 24ºC in vegetative areas (70-80% area). The agricultural land (10-20% area), aqua-agricultural (10-20%), and extensive vegetation cover (60-80%) were the major land cover type along this transect with the built-up area being minimal. Thermal profile was more amplified by 2010 with the land built up and grass land having temperatures of 21-23ºC near the origin whereas the vegetation had relatively constant temperatures of 19-20ºC trends. The steepest change took place in 2020 when the temperature profile was much steeper with the range between about 10ºC of the water bodies and 30ºC of the built-up areas (20-30% area). The growth of built-up land with a negligible coverage in 2000 to about 20-30 percent in 2020 was directly linked to a rise of 4-5ºC in temperature in the urbanized areas and water bodies had a cooling effect and a temperature of 15-20ºC lower than the built-up areas.

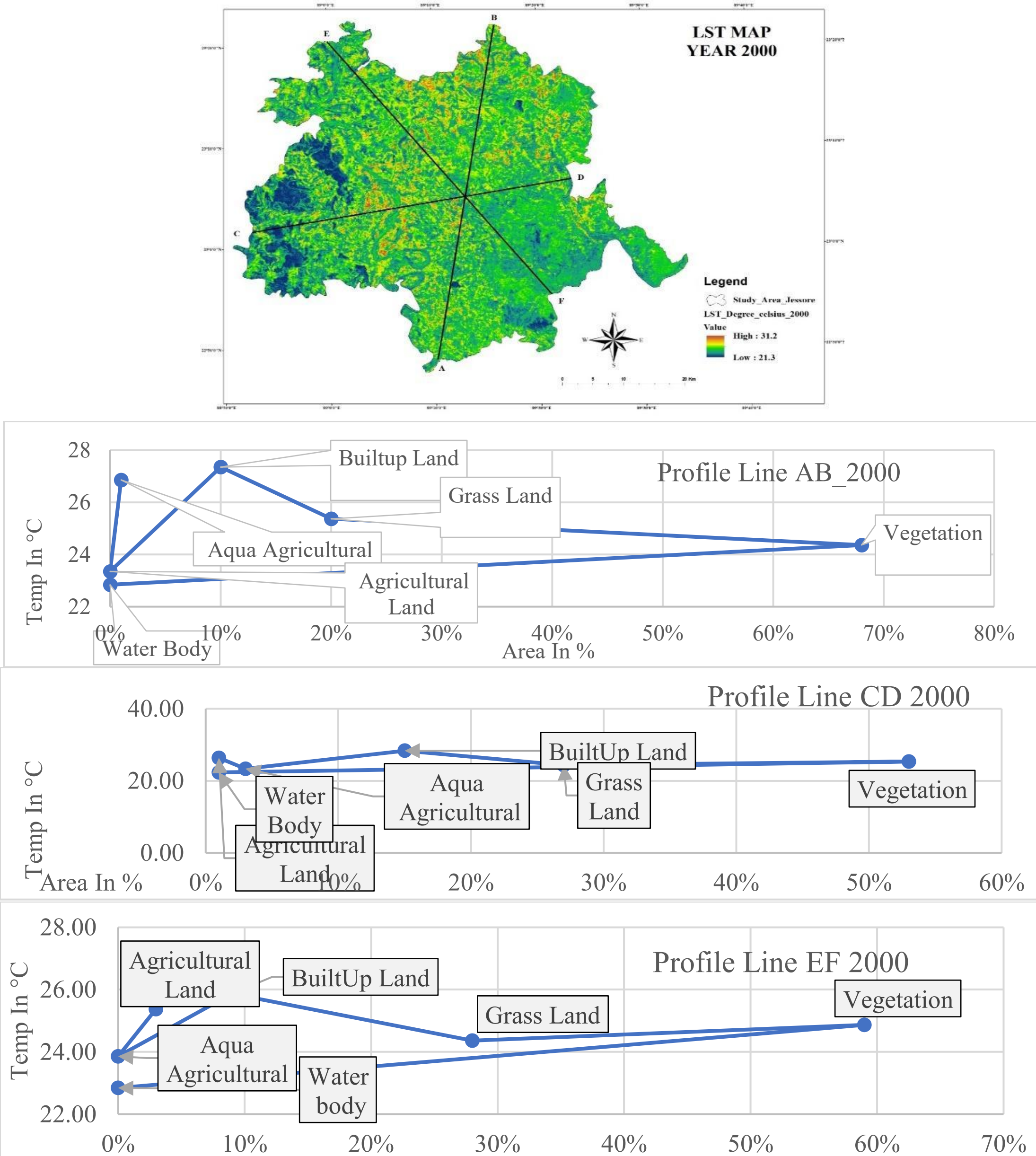


Figure 8: Land Surface Temperature map and profiles with LULC (2000)

### 3.6.2 Profile Line CD Analysis:

The CD transect which is in the central area shows the most significant urban heat island signature. In the year 2000, the temperatures of this profile varied between about 20ºC in water bodies and aqua-agricultural plots (0-10% area) and 27-28ºC in the agricultural land plots (5-15% area) with the built-up land and grass land showing intermediate values of 24-25ºC. Agricultural land had a characterizing land cover (5-15 percent), aqua-agricultural land (10-20 percent), large grass land and vegetation (40-60 percent area). The profile of 2010 indicated high thermal intensifications with water bodies having 20-22ºC whereas built-up land, grass land and herbaceous land (2030 percent area) had temperatures of 22-24ºC. This transect had the highest thermal gradient of any profile line with agricultural land at the origin of the profile with temperatures of 30-35ºC and grass land at the terminus (near 100 percent cumulative area) with a temperature of about 20ºC. Such a 15deg C difference in temperature in a single transect highlights the extreme thermal fragmentation caused by land cover heterogeneity. The polarization of thermal landscape between the urban and rural landmasses can be observed in the reduction in aqua-agricultural dominance in 2000 and the increase in built-up space (0-20% area) and vegetation cover (80-100% area) in 2020.

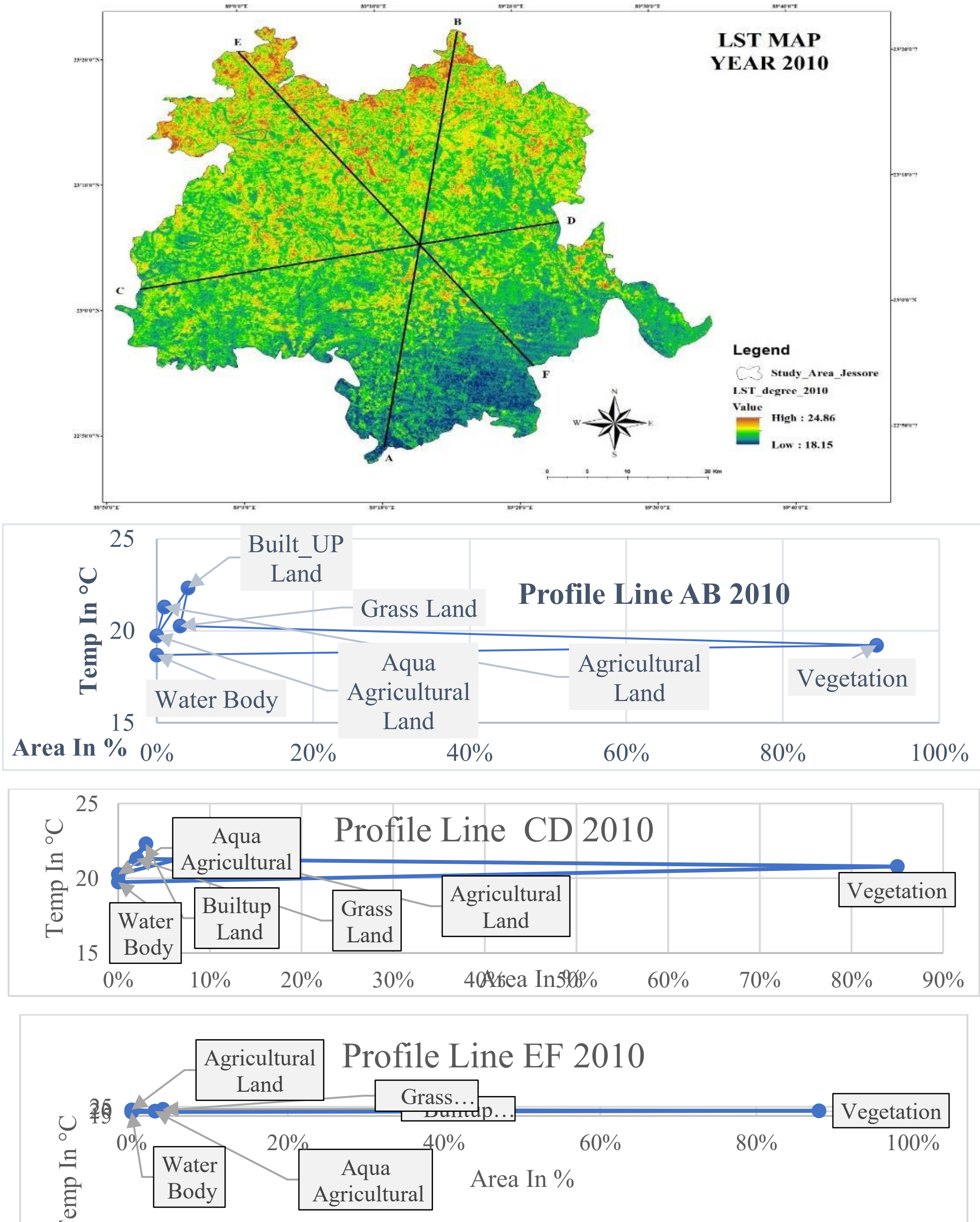


Figure 9: Land Surface Temperature map and profiles with LULC (2010)

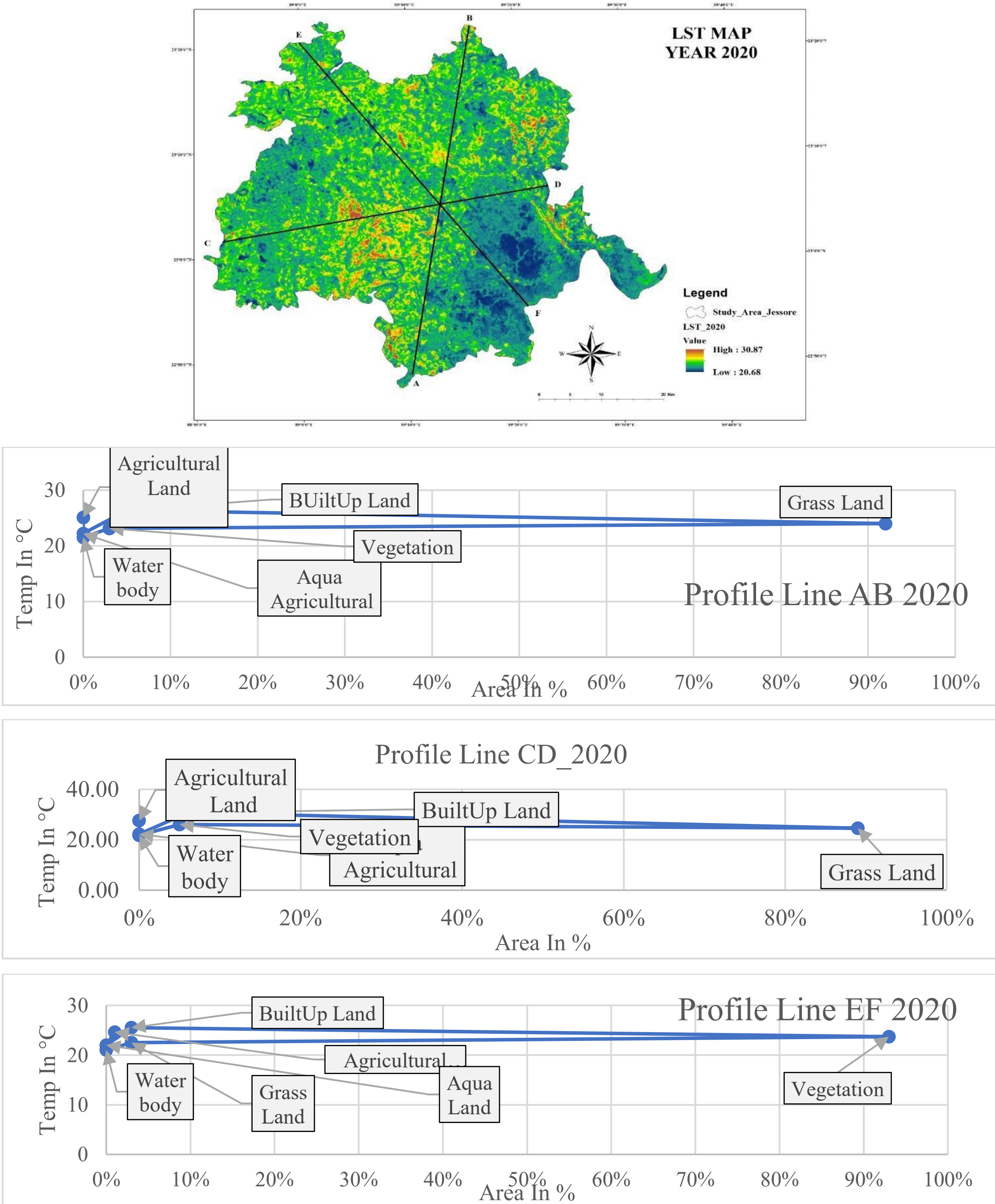


Figure 10. Land Surface Temperature map and profiles with LULC (2020)

### 3.6.3 Profile Line EF Analysis:

The profile EF that was passing through the southern sector showed different thermal characteristics than transects AB and CD. In 2000, temperatures were observed to be 22-23ºC in agricultural land and aqua-agricultural land (0-10% area) up to 25- 26ºC in grass land (30-40% area), and vegetation were kept at 24-25ºC (60-70% area). The temperature range (3-4ºC) was relatively compressed in 2000 which was an indication of thermally homogeneous landscape. In 2010, water bodies (0-5% area) were found at 18-19ºC with aqua-agricultural zones at 19-20ºC and the vegetation at almost 100% cumulative area at around 18ºC, indicating that water bodies and vegetation had a greater cooling impact. Nonetheless, 2020 data indicated that the thermal pattern was complex with water bodies (0-5% area), built-up land (10-20% area) and maximum temperature of 28-30ºC, grass land and agricultural areas at 20-25ºC and vegetation (80-100% area) at 23-25ºC. The appearance of separate thermal peaks which are attributed to the developed areas portrays the intrusion of urban growth in the formerly agricultural regions.

### 3.7 Comparative Temporal Analysis:

Comparative analysis based on the three periods shows that there is a systematic thermal increase. Mean LST rose to 26ºC in 2010 and 28ºC in 2020 with a decadal warming rate of 2ºC, up by about 24ºC in 2000. It also became clear that the standard deviation of the values of LST was greater in 2020 (5-7ºC) than it was in 2000 (2-3ºC) which means that thermal heterogeneity was enhanced. Water bodies continuously recorded the lowest temperatures in all the years (10-22ºC), which was the important thermal buffer whereas built-up areas recorded the highest temperatures (26-35ºC by 2020). Agricultural land exhibited moderate thermal conductivity, and the temperature range was 24-27ºC in 2000 to 28-32ºC in 2020 indicating less soil moisture and vegetation cover. The vegetation zones that covered 60-80% of the profile areas in 2000 dropped to 20-40% in 2020 and this was accompanied by a 3-4ºC temperature rise in turned areas.

### 3.8 Urban Climate and Sustainability implications:

These results play crucial roles in the urban climate resilience and sustainable development planning in Jessore. The rapid rise in LST is especially after 2010, which is accompanied with fast urbanization and development of infrastructure. The heat stress experienced on constructed surfaces creates health hazards during heat waves, makes cooling systems use more energy and makes air quality problems worse. The cooling ability of the water bodies (10-15ºC below the cities) and vegetation (4-6ºC below) show that there is a need to conserve and increase the blue-green infrastructure. Urban forestry, green roof, permeable pavement, and restoration of water bodies are some of the strategic interventions that would reduce the thermal effects by 3-5ºC. The profile line analyses have shown that urban landscapes can be improved in terms of cooling by ensuring that the cool islands (water bodies and vegetation) stay connected with each other via ecological corridors. The future urban development should consider thermal issues by enforcing zoning laws, which presuppose that vegetation percentage should be minimum, the ratio of impervious surface should be limited as well as the water bodies existing at the specific moment should be safeguarded to avoid further deterioration of the thermal conditions and to provide the environmental sustainability.

## 4 Conclusion

We compared the propensity of the changes in LULC and LST fluctuations in Bangladesh's Jessore district, according to the Landsat Image of the area in 2000, 2010, and 2020. As it was found out, in 2000 to 2020 where the urban area grew by 57 km2, but the area under vegetation 362 km2 in total decreased. LST shows a steeply increasing trend in the urban zones and it shows a decreasing trend close to bodies of water. The maximum LST increased by 3ºC in the last 20 years. 21 percent of the area recorded temperatures of 31ºC to 32ºC in the year 2020. It's crucial to remember that the significant component that affects changes in LULC and subsequent increase in LST is urban area development, which is happening at a tremendous rate. Having analysed and classified our study area we learnt that the process of urbanization is directly proportional to the temperature since the barren land is the reason why the temperatures increase three times. Consequently, we came up with a conclusion out of this research that agricultural land and green space are what regulate and maintain the temperature of the atmosphere. Conversely, preventing explosive urban development is difficult unless the program on decentralization is large-scale. A huge increase in LST may damage the components of the ecosystems and health of human beings. Rapid urbanization in the city and the development of LST can be considered by the engineering professionals, urban planners and local administration of Jessore based on the result of this study. The outcomes also provide the urban planners with up-to-date information and an enhanced understanding that will enable them to formulate inclusive urban planning policies and make them more habitable and long-term viability.

# 5 References

Akomolafe, G.F. and Rosazlina, R., 2022. Land use and land cover changes influence the land surface temperature and vegetation in Penang Island, Peninsular Malaysia. Scientific Reports, 12(1), p.21250, DOI: 10.1038/s41598-022-25560-0.

Bao, T., Li, X., Zhang, J., Zhang, Y. and Tian, S., 2016. Assessing the distribution of urban green spaces and its anisotropic cooling distance on urban heat island pattern in Baotou, China. ISPRS International Journal of Geo-Information, 5(2), p.12, DOI: 10.3390/ijgi5020012.

Churches, C.E., Wampler, P.J., Sun, W. and Smith, A.J., 2014. Evaluation of forest cover estimates for Haiti using supervised classification of Landsat data. International Journal of Applied Earth Observation and Geoinformation, 30, pp.203-216, DOI: 10.1016/j.jag.2014.01.020.

Chen, X.L., Zhao, H.M., Li, P.X. and Yin, Z.Y., 2006. Remote sensing image-based analysis of the relationship between urban heat island and land use/cover changes. Remote sensing of environment, 104(2), pp.133-146, DOI: 10.1016/j.rse.2005.11.016.

Fan, C., Myint, S.W., Kaplan, S., Middel, A., Zheng, B., Rahman, A., Huang, H.P., Brazel, A. and Blumberg, D.G., 2017. Understanding the impact of urbanization on surface urban heat islands—A longitudinal analysis of the oasis effect in subtropical desert cities. Remote Sensing, 9(7), p.672, DOI: 10.3390/rs9070672.

Feng, Y., Li, H., Tong, X., Chen, L. and Liu, Y., 2018. Projection of land surface temperature considering the effects of future land change in the Taihu Lake Basin of China. Global and Planetary Change, 167, pp.24-34, DOI: 10.1016/j.gloplacha.2018.05.007.

Ghebrezgabher, M.G., Yang, T., Yang, X., Wang, X. and Khan, M., 2016. Extracting and analyzing forest and woodland cover change in Eritrea based on landsat data using supervised classification. The Egyptian Journal of Remote Sensing and Space Science, 19(1), pp.37-47, DOI: 10.1016/j.ejrs.2015.09.002.

Herold, M., Goldstein, N.C. and Clarke, K.C., 2003. The Spatiotemporal Form of Urban Growth: Measurement, Analysis and Modeling. Remote Sensing of Environment, 86, 286-302. https://doi.org/10.1016/S0034-4257(03)00075-0

Hua, A.K. and Ping, O.W., 2018. The influence of land-use/land-cover changes on land surface temperature: a case study of Kuala Lumpur metropolitan city. European Journal of Remote Sensing, 51(1), pp.1049-1069, DOI: 10.1080/22797254.2018.1542976.

Kafy, A.A., Ferdous, L., Faisal, A.A., Khan, H.A.H. and Sheel, P.K., 2018, March. Exploring the association of surface water body change and rapid urbanization in Rajshahi city Corporation (RCC) area using RS and GIS. In 1st National Conference on Water Resources Engineering (NCWRE 2018).

Kafy, A.A., Islam, M., Khan, A., Ferdous, L. and Hossain, M., 2019. Identifying most influential land use parameters contributing reduction of surface water bodies in Rajshahi city, Bangladesh: a remote sensing approach. Remote Sensing of Land, 2(2), pp.87-95, DOI: 10.21523/gcj1.18020202.

Kamran, K.V., Pirnazar, M. and Bansouleh, V.F., 2015, June. Land surface temperature retrieval from Landsat 8 TIRS: comparison between split window algorithm and SEBAL method. In Third international conference on remote sensing and geoinformation of the environment (RSCy2015) (Vol. 9535, pp. 11-22). SPIE.

Kumar, K.S., Bhaskar, P.U. and Padmakumari, K., 2012. Estimation of land surface temperature to study urban heat island effect using Landsat ETM+ image. International journal of Engineering Science and technology, 4(2), pp.771-778.

Kumar, D. and Shekhar, S., 2015. Statistical analysis of land surface temperature–vegetation indexes relationship through thermal remote sensing. Ecotoxicology and environmental safety, 121, pp.39-44, DOI: 10.1016/j.ecoenv.2015.07.004.

Mallick, J., Rahman, A. and Singh, C.K., 2013. Modeling urban heat islands in heterogeneous land surface and its correlation with impervious surface area by using night-time ASTER satellite data in highly urbanizing city, Delhi-India. Advances in Space Research, 52(4), pp.639-655, DOI: 10.1016/j.asr.2013.04.025.

Minnett, Peter J., and Ian J. Barton. 2009. "Remote Sensing of the Earth's Surface Temperature." Experimental methods in the physical sciences, pp. 333–91. https://doi.org/10.1016/s1079-4042(09)04306-9.

Neteler, M., 2010. Estimating daily land surface temperatures in mountainous environments by reconstructed MODIS LST data. Remote sensing, 2(1), pp.333-351, DOI: 10.3390/rs1020333.

Roy, D. P., et al. Characterization of Landsat-7 to Landsat-8 reflective wavelength and normalized difference vegetation index continuity. 2016. Remote Sensing of Environment, vol. 185, pp. 57–70. https://doi.org/10.1016/j.rse.2015.12.024.

Sholihah, R.I. and Shibata, S., 2019, November. Retrieving spatial variation of land surface temperature based on Landsat OLI/TIRS: a case of southern part of Jember, Java, Indonesia. IOP conference series: earth and environmental science (Vol. 362, No. 1, p. 012125). In. IOP Publishing, DOI: 10.1088/1755-1315/362/1/012125.

Thakur, S., Maity, D., Mondal, I., Basumatary, G., Ghosh, P.B., Das, P. and De, T.K., 2021. Assessment of changes in land use, land cover, and land surface temperature in the mangrove forest of Sundarbans, northeast coast of India. Environment, Development and Sustainability, 23, pp.1917-1943, DOI: 10.1007/s10668-020-00656-7.

Verburg, P.H. and Overmars, K.P., 2009. Combining top-down and bottom-up dynamics in land use modeling: exploring the future of abandoned farmlands in Europe with the Dyna-CLUE model. Landscape ecology, 24, pp.1167-1181, DOI: 10.1007/s10980-009-9355-7.

Wadduwage, S., Millington, A., Crossman, N.D. and Sandhu, H., 2017. Agricultural land fragmentation at urban fringes: an application of urban-to-rural gradient analysis in Adelaide. Land, 6(2), p.28, DOI: 10.3390/land6020028.

Weng, Q., 2001. A remote sensing? GIS evaluation of urban expansion and its impact on surface temperature in the Zhujiang Delta, China. International journal of remote sensing, 22(10), pp.1999-2014.

Wondrade, N., Dick, Ø.B. and Tveite, H., 2014. GIS based mapping of land cover changes utilizing multi-temporal remotely sensed image data in Lake Hawassa Watershed, Ethiopia. Environmental monitoring and assessment, 186, pp.1765-1780, DOI: 10.1007/s10661-013-3491-x.

Xiao, H. and Weng, Q., 2007. The impact of land use and land cover changes on land surface temperature in a karst area of China. Journal of environmental management, 85(1), pp.245-257, DOI: 10.1016/j.jenvman.2006.07.016.

Yuan, F., Sawaya, K.E., Loeffelholz, B.C. and Bauer, M.E., 2005. Land cover classification and change analysis of the Twin Cities (Minnesota) Metropolitan Area by multitemporal Landsat remote sensing. Remote sensing of Environment, 98(2-3), pp.317-328, DOI: 10.1016/j.rse.2005.08.006.

Zhang, H., Qi, Z.F., Ye, X.Y., Cai, Y.B., Ma, W.C. and Chen, M.N., 2013. Analysis of land use/land cover change, population shift, and their effects on spatiotemporal patterns of urban heat islands in metropolitan Shanghai, China. Applied Geography, 44, pp.121-133, DOI: 10.1016/j.apgeog.2013.07.021.